ARTICLE | Article in Press

Anti-GD2 CAR T cells efficiently target Ewing's sarcoma

Giulia Golinelli · Chiara Chiavelli · Malvina Prapa · Marco Silingardi · Leonardo Brini · Giuseppe Pugliese · Giovanni Neri · Carlotta Spano · Rosanna Di Tinco · Laura Bertoni · Riccardo Cuoghi Costantini · Giulia Rovesti · Alice Morellini · Tiziana Petrachi · Jonathan Vinet · Marco Bestagno · Maria Cristina Baschieri · Federico Banchelli · Giovanni Palazzi · Edwin M. Horwitz · Bruce L. Levine · Massimo Dominici

Received: 8 November 2025 / Revised: 24 August 2026 / Accepted: 2 September 2026
© The Author(s) 2026

Abstract

Ewing's sarcoma (ES) is an aggressive cancer primarily affecting children and young adults. Although chimeric antigen receptor (CAR) T cell therapy has achieved remarkable success in hematologic malignancies, its efficacy against solid tumors such as ES remains limited. Our previous studies demonstrated the therapeutic potential of GD2 CAR T cells against brain tumors and showed that a truncated GD2 CAR enhances the tumor-targeting ability and antitumor efficacy of mesenchymal stromal/stem cells against metastatic ES. Here, we further investigated the therapeutic potential of GD2 CAR T cells in ES, a disease for which effective treatment options remain a significant unmet medical need. The antitumor activity of GD2 CAR T cells was assessed using different two-dimensional and three-dimensional in vitro ES models and an in vivo ES xenograft model. GD2 CAR T cells effectively killed ES cells in both two-dimensional and three-dimensional settings, including an ES cell line displaying low GD2 expression. In vivo, GD2 CAR T cells efficiently targeted localized ES tumors and counteracted tumor growth. CAR T cells infiltrated the tumors and were also detected in the blood and spleen of treated mice. Overall, these findings support the efficacy of GD2 CAR T cells against both in vitro models and a localized in vivo model of ES. These findings underscore the potential of GD2 CAR T cell-based therapies to improve treatment outcomes in ES and other lethal GD2-positive malignancies.

Introduction

Ewing's sarcoma (ES) is an aggressive tumor and the second most common bone or soft-tissue cancer in children and young adults [1]. Conventional chemotherapy, while offering favorable cure rates for localized ES, is associated with substantial late effects. Conversely, patients with metastatic or recurrent ES face dismal outcomes, despite receiving complex treatment regimens that include surgery, radiotherapy, and chemotherapy [2]. There is a critical and urgent need for novel treatment strategies to improve the quality of cure for localized disease and to enhance survival rates for metastatic or recurrent ES [3]. Novel agents, that can target resistant clones and deliver drugs more precisely to minimize side effects, represent promising approaches to be combined with standard treatments.

Our previous works have demonstrated the potential of using a mesenchymal stromal/stem cell (MSC)-based strategy to counteract localized ES, employing MSCs to deliver the tumor necrosis factor-related apoptosis-inducing

This Article in Press is shared early to give you faster access to new research. It is citable and carries a permanent DOI. The final edited version will replace it automatically.

Published online: 03 November 2026

ligand (TRAIL) [4]. More recently, we enhanced the tumor-targeting capacity of MSC-TRAIL by introducing a truncated chimeric antigen receptor (tCAR) directed against the disialoganglioside GD2, with the aim of targeting metastatic disease [5]. CAR-modified T cells have opened new avenues of research, demonstrating therapeutic success in hematological malignancies [6]. However, clinical responses in solid tumors remain limited, with a few notable exceptions, such as IL-13Rα2-targeted CAR T cells in glioblastoma and GD2-specific CAR T cells in pediatric midline gliomas. Larger studies have reported encouraging results with claudin18.2-targeted CAR T cells in gastrointestinal tumors [7].

Sarcomas have recently emerged as promising targets for engineered T cell therapies, as highlighted by the FDA approval of the T cell receptor (TCR) gene therapy afamitresgene autoleucel (Tecelra) for unresectable or metastatic synovial sarcoma [8], a tumor known for its sensitivity to immunomodulation [9]. In contrast, ES is characterized by poor T lymphocyte infiltration and a low immune-active tumor microenvironment (TME), consistent with its low tumor mutational burden [10]. Notably, higher numbers of tumor-infiltrating $CD8^+$ T cells have been associated with better prognosis in ES patients, suggesting that enhancing immune cell recruitment, either spontaneously or through adoptive transfer, may be critical for effective anti-tumor responses [11, 12].

Preclinical CAR T cell studies in ES have explored multiple targets, including vascular endothelial growth factor receptor 2 (VEGFR2), insulin-like growth factor 1 receptor (IGF1R), receptor tyrosine kinase-like orphan receptor 1 (ROR1), B7-H3, hepatocellular receptor tyrosine kinase (EphA2), natural killer group 2D (NKG2D) and GD2 [13]. Among these, GD2 represents one of the most promising targets due to its high expression on tumor cells, limited distribution in normal tissues, and accumulating clinical evidence supporting the safety of GD2 CAR T cell therapies [14–16]. GD2 expression has been consistently reported in ES, both in vitro and in patient-derived tumor samples across different disease stages, including relapse [17]. Despite encouraging in vitro findings, GD2-targeted CAR T or NK cell therapies have shown limited efficacy as monotherapies in controlling tumor growth, particularly in metastatic ES models [17–19]. In this study, we challenged a second-generation GD2.BBz CAR previously used to target neuroblastoma and GBM [20–22], as well as in its truncated form expressed on MSCs for ES and GBM targeting [5, 23].

Here, we confirm the potent anti-tumor activity of our CAR T cell product across several in vitro ES models and an in vivo ES model.

Results

GD2 CAR T cells effectively mediate in vitro anti-tumor activity against ES cells

To assess the effect of GD2 CAR T cells against ES, three ES cell lines displaying different levels of GD2 expression were selected, as we previously reported [5]. These included the $GD2^{high}$ TC71, with GD2 expression in 99.7 ± 0.1% of cells, the $GD2^{low}$ A673 (17.0 ± 10%) and the $GD2^{very\ low}$ RD-ES (1.5 ± 1%) (Supplementary Fig. 1a). This approach enabled the evaluation of GD2 CAR T cell response across a spectrum of GD2 expression levels. The anti-tumor activity of GD2 CAR T cells was first assessed against 2D cultures with ES cell lines. As done with GBM cells [22], ES cell lines were stably transduced with viral vectors encoding a fluorescent reporter (DsRed or mScarlet) together with luciferase for tumor cell monitoring. T cells isolated from healthy donor (HD) peripheral blood mononuclear cells (PBMCs) were engineered with a retroviral vector expressing a second-generation GD2 CAR [20], with a transduction efficiency of 76.3 ± 7.7% (Supplementary Fig. 1b). Of the GD2 CAR T cells, 28.0 ± 19.0% were CD4+ and 70.7 ± 19.2% were CD8+, similar to the proportions in GFP T cells (23.8 ± 17.1% CD4+ and 74.2 ± 16.2% CD8+; Supplementary Fig. 1c). NK and NKT cells in the product accounted for 0.5 ± 0.4% and 7.4 ± 1.8% in GD2 CAR T cells, and 0.8 ± 0.3% and 7.1 ± 2.5% in GFP T cells, respectively (Supplementary Fig. 1c). For γδ T cells, the percentages were 2.0 ± 0.6% in GD2 CAR T cells and similarly 2.1 ± 1.1% in GFP T cells (Supplementary Fig. 1c). GD2 CAR T cells were challenged in co-cultures against tumor cells, testing different time points of 24, 48 and 72 h, multiple effector-to-target ratios (1:1, 2:1, 5:1 E:T ratios), and using different PBMC donors

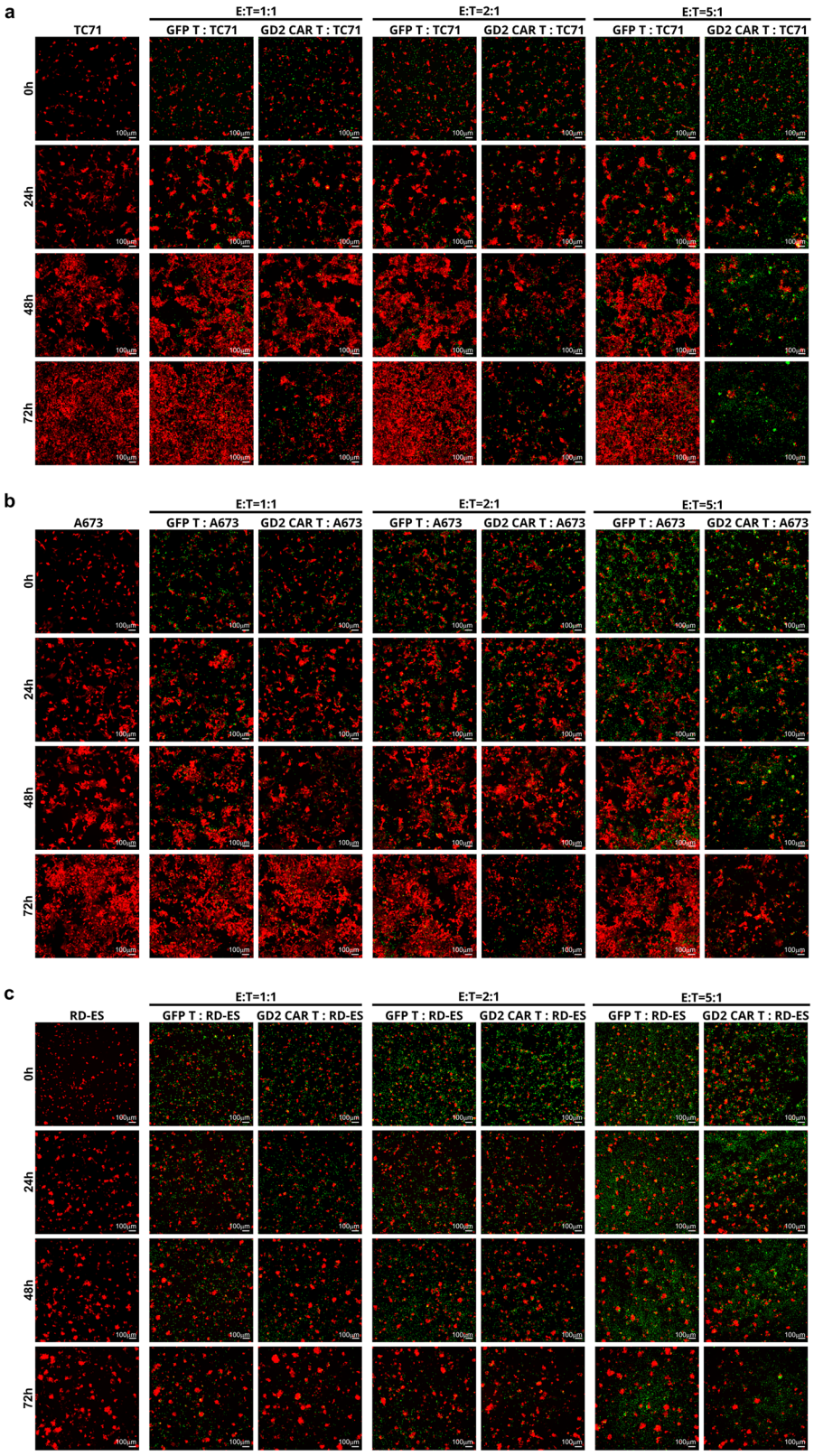


Fig. 1 Representative immunofluorescence images of GD2 CAR T cell co-cultures with ES cell lines. The in vitro impact of GD2 CAR T cells against ES cell lines, with high (TC71), low (A673), and very low (RD-ES) GD2 expression, was evaluated by 2D co-cultures over 72 h. Tumor cells cultured alone and in co-culture with GFP T cells served as controls. Representative fluorescence micrographs of TC71 (**a**), A673 (**b**), and RD-ES (**c**) (all ES cells in red) with GD2 CAR T cells or GFP T cells (in green) at 1:1, 2:1, and 5:1 effector-to-target (E:T) ratios at 0, 24, 48, and 72 h of co-culture. Scale bar: 100 µm.

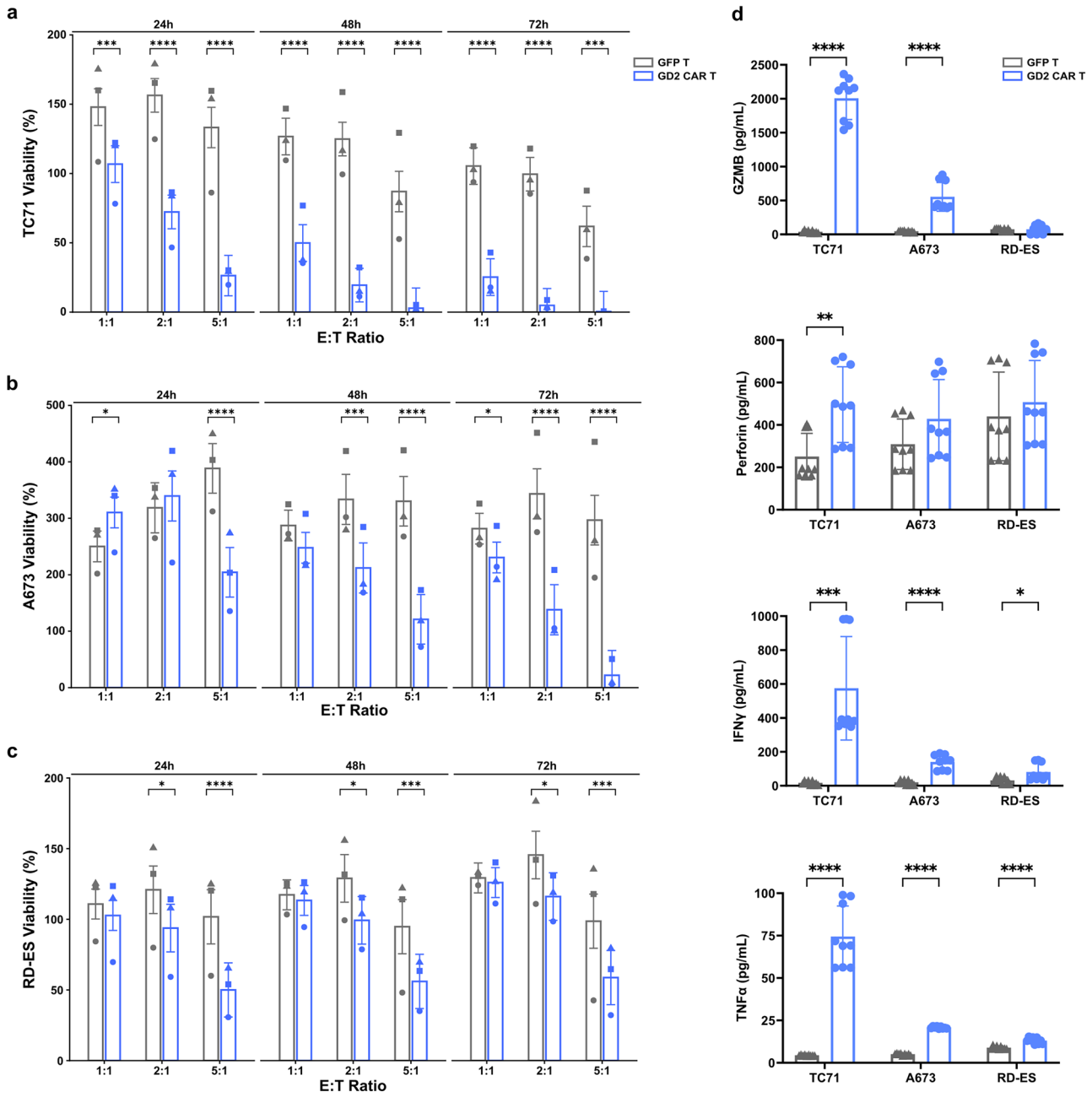


Fig. 2 GD2 expression modulates GD2 CAR T cell cytotoxic activity and cytokine release against Ewing's sarcoma in 2D in vitro models. The in vitro cytotoxic activity of GD2 CAR T cells was evaluated against the ES cell lines TC71, A673, and RD-ES in 2D co-culture assays. Tumor cell viability was assessed by bioluminescence quantification in TC71 (**a**), A673 (**b**), and RD-ES (**c**) at different effector-to-target (E:T) ratios (1:1, 2:1, and 5:1) over 24, 48, and 72 h. **d** Granzyme B (GZMB), perforin, IFNγ, and TNFα levels were assessed in supernatants of co-cultures involving GD2 CAR T cells or control GFP T cells with TC71, A673, or RD-ES cells at 2:1 E:T ratio at 72 h, and concentrations are reported as pg/mL. For panels (**a**–**c**), statistical analysis was performed using linear mixed-effects models with treatment group, time, and their interaction included as fixed effects, and donor and sample ID as random intercepts. Models were fitted using restricted maximum likelihood (REML), and Type III Wald χ^2 tests were used to assess fixed effects and interactions. For panel (**d**), *P*-values were determined by *t*-test and adjusted using the Holm–Šídák method. $*p \le 0.05$; $**p \le 0.01$; $***p \le 0.001$; $****p \le 0.0001$. Data are shown as mean ± SD. Number of independent experiments: $n = 3$ from three different T cell donors, each with six technical replicates (**a**–**c**), and $n = 3$ from three different T cell donors, each with three technical replicates (**d**).

to account for inter-donor variability. GFP T cells were introduced as a control to measure T cells alloreactivity.

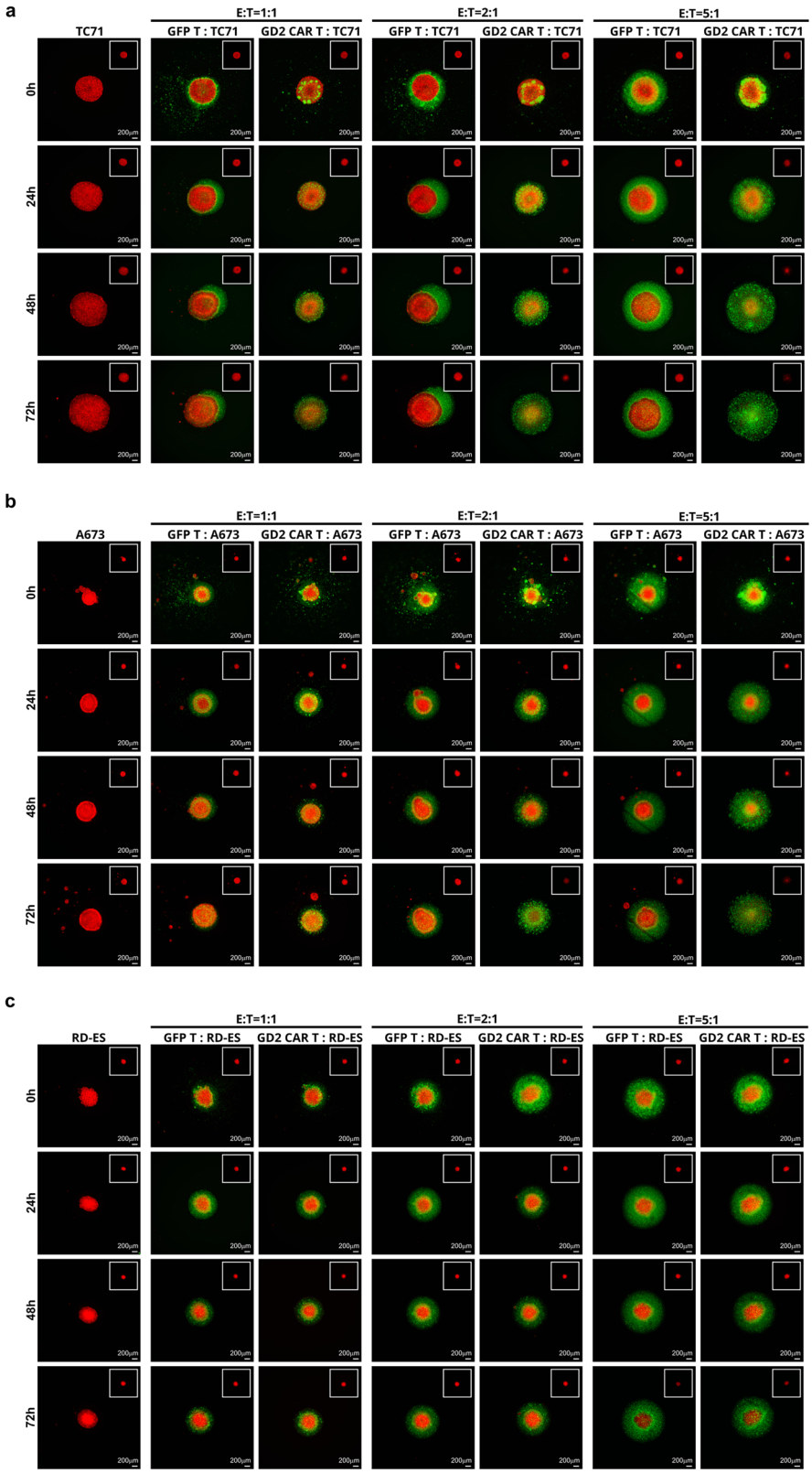


Fig. 3 Representative 3D ES spheroid co-cultures reveal antigen-dependent GD2 CAR T cell activity. Spheroids were monitored by fluorescence microscopy for T cell infiltration and tumor spheroid disruption at 0, 24, 48, and 72 h of co-culture at different effector-to-target (E:T) ratios (1:1, 2:1, and 5:1). Untreated spheroids and GFP T cell-treated spheroids served as controls. Representative fluorescence images of co-cultures between TC71 (**a**), A673 (**b**), and RD-ES (**c**) cell lines (in red) and GD2 CAR T cells and GFP T cells (in green) are shown. Scale bar: 200 µm.

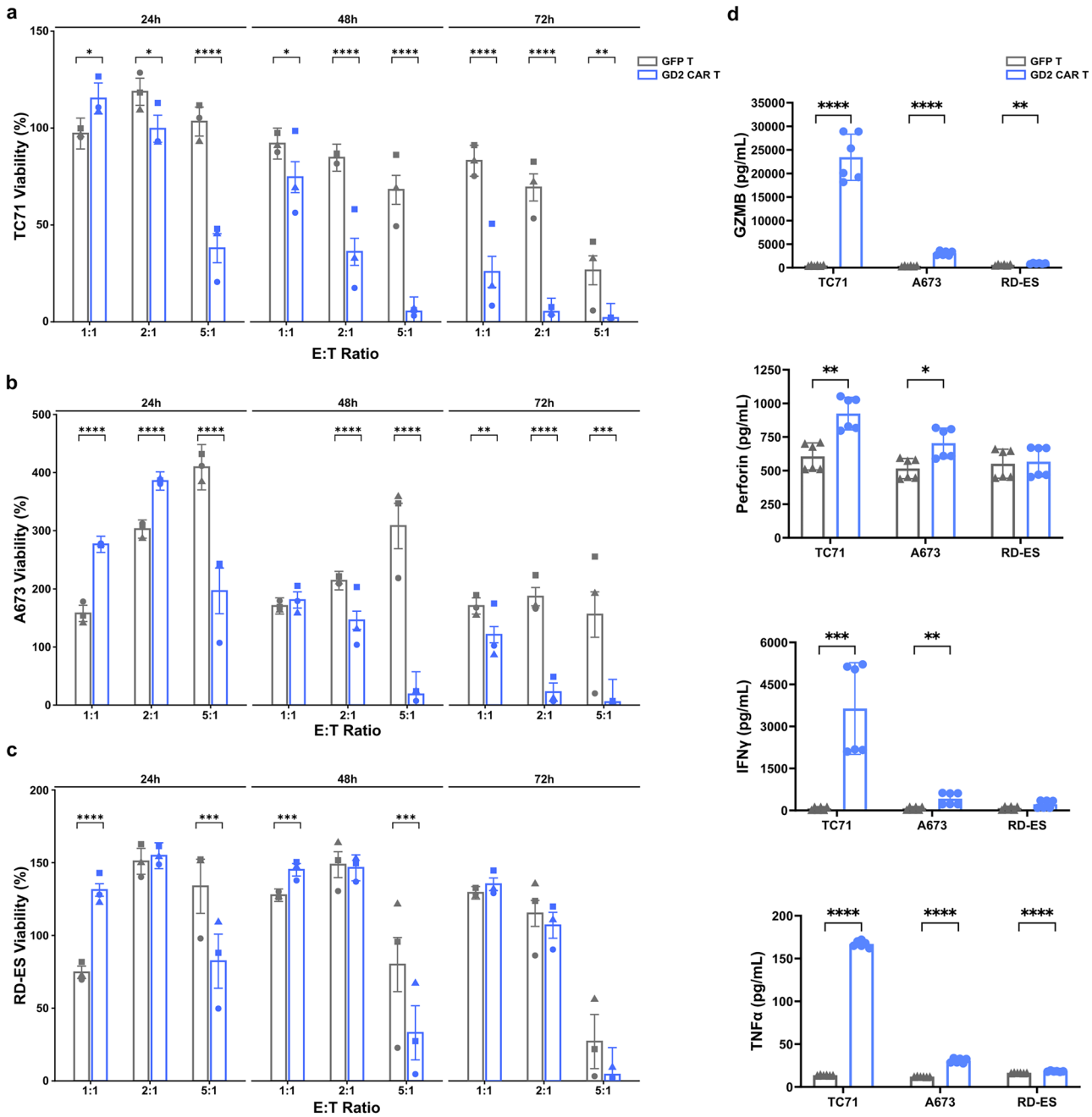


Fig. 4 GD2 expression shapes GD2 CAR T cell anti-tumor activity in 3D ES spheroid models. The in vitro anti-tumor activity of GD2 CAR T cells was assessed in 3D spheroid co-cultures using the ES cell lines TC71, A673, and RD-ES. Tumor cell viability was quantified by bioluminescence at 24, 48, and 72 h using different effector-to-target (E:T) ratios (1:1, 2:1, and 5:1) for TC71 (**a**), A673 (**b**), and RD-ES (**c**). **d** Granzyme B (GZMB), perforin, IFNγ, and TNFα levels were measured in supernatants of co-cultures of GD2 CAR T cells or control GFP T cells with TC71, A673, or RD-ES spheroids at a 2:1 E:T ratio after 72 h, and are reported as pg/mL. For panels (**a**–**c**), statistical analysis was performed using linear mixed-effects models with treatment group, time, and their interaction included as fixed effects, and donor and sample ID as random intercepts. Models were fitted using restricted maximum likelihood (REML), and Type III Wald χ^2 tests were used to assess fixed effects and interactions. For panel (**d**), *P*-values were determined by *t*-test and adjusted using the Holm–Šídák method. *$p \le 0.05$; **$p \le 0.01$; ***$p \le 0.001$; ****$p \le 0.0001$. Data are shown as mean ± SD. Number of independent experiments: $n = 3$ from three different T cell donors, each with six technical replicates (**a**–**c**), and $n = 2$ from two different T cell donors, each with three technical replicates (**d**).

Fluorescence imaging performed up to 72 h across different E:T ratios revealed distinct patterns of response to GD2

CAR T cell treatment. Among the three ES models, the GD2^{high} TC71 cells displayed the most robust response to GD2 CAR T cells, with extensive tumor cell clearance and the formation of reactive T cell clusters (Fig. 1a). In contrast, the GD2^{low} A673 cells showed a detectable anti-tumor response predominantly at the highest 2:1 and 5:1 E:T ratios (Fig. 1b), whereas the GD2$^{very\ low}$ RD-ES cells remained largely unaffected, confirming the antigen-dependent activity of GD2 CAR T cells (Fig. 1c). No comparable cytotoxic effect was observed in GFP T cell control conditions (Fig. 1).

Tumor cell viability, quantified by bioluminescence signal measurements (Fig. 2a–c), further demonstrated that GD2 CAR T-mediated cytotoxicity directly correlated with the level of GD2 antigen expressed on the tumor cell membrane. TC71 cells exhibited the strongest reduction in viability across all tested E:T ratios (Fig. 2a), while A673 cells showed a more modest but significant response at higher effector cell numbers (Fig. 2b). Conversely, the RD-ES line displayed only a minimal, although statistically significant, cytotoxic response at the highest 5:1 E:T ratio, consistent with the very low levels of GD2 expression detected in this cell line (Fig. 2c). To further support the potent antigen-dependent activity of GD2 CAR T cells, we employed an automated single-cell killing assay platform allowing the evaluation of isolated effector cell cytotoxicity at an extremely low E:T ratio (~1:10). Even under these highly unfavorable conditions, GD2 CAR T cells induced a significant increase in TC71 cell death within 24 h, further confirming the strong antigen-dependent killing capability of GD2 CAR T cells (Supplementary Fig. 2).

This antigen-dependent functional activity became even more evident in the cytokine release analysis performed after 72 h of co-culture at the 2:1 E:T ratio. Supernatants collected from co-cultures generated using three independent PBMC donors consistently showed increased secretion of Granzyme B, perforin, IFNγ, and TNFα in GD2 CAR T cell conditions compared to GFP T controls, with cytokine levels closely mirroring the degree of GD2 surface expression and cytotoxic activity observed in each ES cell line (Fig. 2d). Notably, TC71 cells induced the strongest and most complete effector response, particularly in terms of Granzyme B and IFNγ release, whereas A673 cells elicited an intermediate activation profile consistent with lower GD2 expression. Although RD-ES cells displayed minimal cytotoxic sensitivity, low but detectable increases in IFNγ, and TNFα release were still observed, suggesting that even very low GD2 surface levels may partially activate GD2 CAR T cells without promoting efficient tumor killing. Despite expected inter-donor variability, both cytotoxicity and cytokine release profiles demonstrated highly reproducible and robust GD2-specific CAR T cell activation.

GD2 CAR T cell cytotoxic effect is preserved in 3D ES models

The anti-tumor effect of GD2 CAR T cells was further assessed in 3D spheroid models, taking into account the enhanced aggressiveness of cells in a 3D environment and the challenges that CAR T cells may face in penetrating solid tumors [24].

Spheroids generated from the GD2^{high} TC71, GD2^{low} A673, and GD2$^{very\ low}$ RD-ES cell lines were challenged with GD2 CAR T cells and GFP T cell controls at different E:T ratios (1:1, 2:1, and 5:1), and monitored by fluorescence imaging up to 72 h (Fig. 3). Consistent with the observations obtained in 2D co-cultures, TC71 spheroids displayed the strongest sensitivity to GD2 CAR T cell treatment (Fig. 3a). GD2 CAR T cells efficiently infiltrated and progressively disrupted the spheroid architecture even at the lowest 1:1 E:T ratio, leading to a marked reduction in tumor fluorescence and spheroid integrity over time. Increasing E:T ratios further enhanced the anti-tumor effect, with near-complete elimination of the spheroid observed at 72 h in the 5:1 condition (Fig. 3a). A673 spheroids exhibited a delayed but still significant response to GD2 CAR T cells (Fig. 3b). Limited differences between GFP T and GD2 CAR T cells were observed at the 1:1 E:T ratio, whereas a clear GD2 CAR T cell advantage emerged at the 2:1 and 5:1 ratios, particularly at later time points. At 72 h, GD2 CAR T cells markedly disrupted spheroid compactness and reduced tumor fluorescence intensity, while GFP T-treated spheroids retained a more preserved fluorescent tumor core (Fig. 3b). Conversely, RD-ES spheroids did not show evident morphological differences between GD2 CAR T and GFP T-treated conditions throughout the assay, even at the highest 5:1 E:T ratio after 72 h (Fig. 3c).

The qualitative imaging observations were further confirmed by bioluminescence-based viability quantification (Fig. 4a–c). TC71 spheroids showed the strongest reduction in viability across all tested E:T ratios and time points

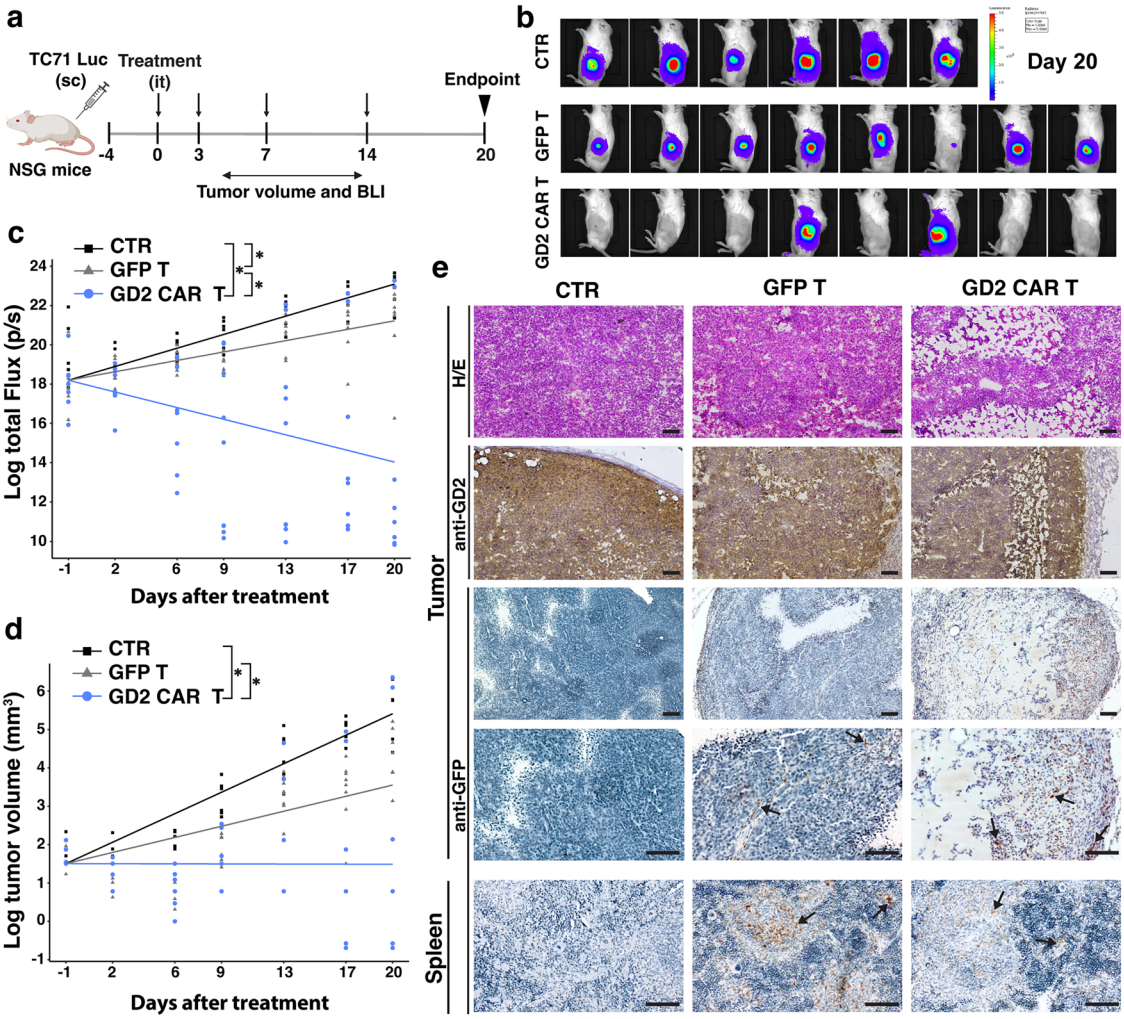


Fig. 5 GD2 CAR T cell therapy controls tumor growth and achieves remission in most mice with localized ES model. **a** Schematic of in vivo mouse experiments evaluating the anti-tumor efficacy of GD2 CAR T cells in a localized subcutaneous (sc) ES model. GD2 CAR T cells were administered intra/peri-tumorally four days after tumor cell injection (day 0) and on days 3, 7, and 14 after the first CAR T cell dose. The study endpoint was day 20 post-CAR T cell injection. **b** Tumor bioluminescence at endpoint was measured using the IVIS Lumina XRMS with Living Image software. Total flux (photons/s; **c**) and tumor volume (mm^3; **d**) of GD2 CAR T cell-treated (GD2 CAR T), GFP T cell control-treated mice (GFP T), and control animals (CTR) were monitored by IVIS Lumina XRMS system and calliper measurement, respectively. **e** Photomicrographs of representative tumor samples on day 20 stained for H/E (first row), anti-GD2 antibody to detect GD2-positive tumor cells (second row), and anti-GFP antibody to visualize GFP-positive adoptively transferred human T cells (third and fourth row; black arrows) by IHC. Images shown at 20X (fourth row) represent magnified views of the corresponding 10X fields (third row). Spleens were also stained to detect GFP-positive human T cells (fifth row; black arrows). Scale bars: 100 µm. *P*-value ($*p \le 0.05$) were calculated by mixed-effects model with a Gamma distribution and a logarithmic link. Data are shown in logarithmic form. Number of independent experiments $n = 1$, from one T cell donor. $N = 6$ mice/group for CTR, and $n = 8$ mice/group for both GD2 CAR T and GFP T groups.

(Fig. 4a), whereas A673 spheroids displayed a more moderate, but significant decrease in viability, particularly at higher E:T ratios and longer co-culture times (Fig. 4b). In contrast, RD-ES spheroids did not show a significant killing advantage of GD2 CAR T over GFP T cells across the tested conditions (Fig. 4c). At the highest 5:1 E:T ratio, both GD2 CAR T and GFP T cells induced a comparable reduction in spheroid viability, consistent with an alloreactive effect.

To further characterize GD2 CAR T cell activation within the 3D model, cytokine release was evaluated after 72 h of co-culture at the 2:1 E:T ratio (Fig. 4d). In agreement with both imaging and viability data, GD2 CAR T cells co-

cultured with TC71 and A673 spheroids released significantly higher levels of Granzyme B, perforin, IFNγ, and TNFα compared to GFP T controls, with TC71 spheroids inducing the strongest cytokine response overall. Conversely, RD-ES spheroids elicited minimal cytokine production, further supporting the dependence of CAR T activation and cytotoxic activity on GD2 antigen density.

Collectively, these findings demonstrate that GD2 CAR T cells retain potent and antigen-dependent anti-tumor activity even in complex 3D ES models, supporting their further evaluation in vivo.

GD2 CAR T cells exert anti-tumor activity in an ES in vivo model

The anti-tumor effect of adoptively transferred GD2 CAR T cells against ES was evaluated in a subcutaneous in vivo model using the highly GD2-positive TC71 cell line (Fig. 5a). Mice were randomized into three groups, control (CTR), GFP T, and GD2 CAR T, which were treated with PBS, GFP T cells, and GD2 CAR T cells, respectively. Upon detection of palpable tumors, mice were treated with four peri/intra-tumoral doses of their assigned treatment (PBS, GFP T cells, or GD2 CAR T cells) over a period of two weeks. Comparing groups by tumor bioluminescence at the day 20 endpoint, a superior anti-tumor effect in the GD2 CAR T group was observed, with 5 out of 8 mice showing no detectable tumor, 1 where tumor growth was controlled and only 2 outliers where mice had escaped treatment (Fig. 5b). By day 20 after CAR T cell injection, the tumor-related bioluminescence signal significantly dropped in the GD2 CAR T group (percentage change per day −15.7%, 95% CI: −22.9% to −7.7%, p-value < 0.001, Fig. 5c). Bioluminescence decreased an average of 15.7% per day. For the CTR and GFP T groups, on average, the bioluminescence increased by 39.1% (95% CI: 24.6% to 53.7%, p-value < 0.001) per day compared to the GD2 CAR T group. Overall, with increasing time, the average volume in the GD2 CAR T group did not change significantly (percentage change per day +3.0%, 95% CI: −1.0% to +7.3%, p-value = 0.110). Conversely, in the CTR group, the volume increases by 18.5% (95% CI: 12.7–23.4%, p-value < 0.001) more per additional day compared to the GD2 CAR T group. Finally, in the GFP T group, the volume increases by an average of 11.6% (95% CI: 6.2–16.2%, p-value < 0.001) more per additional day compared to the GD2 CAR T group (Fig. 5d). The GFP T group exhibited a growth in tumor volume lower than that of the CTR condition: in the CTR, the volume increases on average by 5.8% (95% CI: 2.0–10.5%, p-value = 0.007) more per day, compared to what is observed in the GFP T group.

GD2 expression was confirmed by IHC on tumor masses collected at the experimental endpoint (Fig. 5e), as well as on tumor cells after tumor dissociation or short-term culture (not shown). High GD2 expression was maintained across all treatment groups, including tumors from outlier mice that escaped GD2 CAR T cell treatment, with no significant differences among groups, arguing against tumor antigen loss as a mechanism of resistance in our model.

GFP immunostaining further demonstrated the presence of T cells, including GD2 CAR T cells, within and surrounding tumor masses, as well as in the spleens (Fig. 5e). Notably, GD2 CAR T cells were also detected in tumors that escaped CAR T cell treatment, indicating that tumor progression occurred despite CAR T cell infiltration and persistence within the tumor microenvironment. Collectively, these findings suggest that resistance in escaping tumors is unlikely to be driven by antigen loss or defective CAR T-cell trafficking, but rather by functional resistance mechanisms.

Discussion

While CAR T cell therapy has shown remarkable efficacy in treating hematological malignancies, its application to solid tumors remains in the early stages of development with limited efficacy [6]. This study contributes to assessing innovative therapeutic strategies in treating ES, a rare tumor that continues to have a poor prognosis, especially in its metastatic and recurrent forms [3]. Emerging immunotherapies, such as adoptive CAR T cell therapy, hold promise for opening new research avenues by addressing the scarcity of tumor-specific T cell clones and activating the TME [25, 26]. The ganglioside GD2 remains an attractive target in ES, especially considering safety data from recently completed and ongoing early-phase clinical trials on GD2-expressing neuroblastoma and midline gliomas [14, 27].

These trials underscore the significance of GD2 as a clinically relevant tumor-associated antigen, suggesting its potential value in the treatment of ES. ES is susceptible to targeted therapies due to its dependence on specific fusion proteins, primarily the EWS-FLI1 protein, resulting from t(11:22) translocations. However, the translation of inhibitory compounds or oligonucleotides into clinical settings has been hindered by toxicity or low bioavailability, thereby demanding the exploration of novel therapeutic strategies [28]. Immunologically, ES is characterized as a cold tumor with minimal immune or inflammatory cell infiltration, due to immune escape, immune privilege, or immune suppression by the TME [25]. GD2-directed CAR-modified T and NK cells were shown to effectively kill GD2-expressing ES tumor cells in 2D and 3D models and demonstrated substantial anti-tumor efficacy in a localized xenograft model of ES in immunodeficient mice [17–19]. Nevertheless, the effectiveness of GD2 CAR T cells as a monotherapy in ES, especially in metastatic or recurrent forms, remains limited [13].

Importantly, our study does not simply confirm the feasibility of targeting GD2 in ES, which has been previously reported [17–19], but further extends the characterization of GD2 CAR T cell activity using a distinct second-generation GD2.BBz CAR construct incorporating a proprietary anti-GD2 scFv (clone 126), different from the commonly used 14G2a-derived CARs previously investigated in ES models [17, 18, 20]. Our work systematically evaluates CAR T cell activity across tumor models displaying distinct levels of GD2 expression, including ES cell lines with high, low, and very low GD2 expression, allowing a direct assessment of the relationship between antigen density and CAR T cell efficacy.

In our 2D co-cultures, we confirmed the cytotoxic activity of our GD2 CAR T cell product against the $GD2^{high}$ TC71 cells, as well as the $GD2^{low}$ A673 line. By fluorescent microscopy, quantification of tumor cell killing and cytokine release, we observed a superior anti-tumor response of GD2 CAR T cells compared to GFP T cells, confirming specific activation of lymphocytes after CAR-mediated antigen engagement, coupled with a significant release of anti-cancer cytotoxic molecules, as we previously demonstrated in GBM [22]. No clear effects resulted from the co-culture of GD2 CAR T cells and GFP T cells with the $GD2^{very\ low}$ RD-ES cell line, further indicating the selective targeting of GD2-expressing tumor cells by GD2 CAR T cells.

Moving to 3D tumor spheroid models which better emphasize the challenge of targeting a solid tumor [24], GD2 CAR T cells significantly disrupted the TC71 highly GD2-positive spheroid structure and reduced tumor viability, even at a low E:T ratio. GD2 CAR T cells exhibited anti-tumor activity even against the $GD2^{low}$ A673 spheroids. The GD2 CAR-mediated effect was particularly pronounced at the highest E:T ratio, where GD2 CAR T cells completely eradicated the TC71 and A673 tumor spheroids, respectively.

Importantly, cytokine release analyses performed in both 2D and 3D models showed highly consistent activation profiles, further supporting the antigen-dependent functional activity of GD2 CAR T cells. Increased secretion of Granzyme B, perforin, IFNγ, and TNFα closely mirrored the degree of GD2 expression and tumor cell killing, with TC71 models eliciting the strongest effector response, followed by the intermediate $GD2^{low}$ A673 cells, while the $GD2^{very\ low}$ RD-ES model induced only minimal cytokine production. The preservation of this functional activation profile in 3D spheroids further supports the ability of GD2 CAR T cells to remain active in more complex tumor settings, that better recapitulate solid tumor architecture.

Further confirmation was obtained in a localized ES in vivo model, where complete regression in most treated mice was observed following treatment with GD2 CAR T cells. These results align with a previous report [17], although higher doses of CAR T cells were employed in those investigations and a complete regression was apparently not obtained. In contrast, mice in the GFP T cell and in the CTR groups showed a steady increase in the tumor mass instead. This relevant therapeutic benefit underscores the potential of GD2 CAR T cell therapy as a viable approach for the management of ES. While our approach has a limit in a local intra-tumoral injection, it is in line with emerging neoadjuvant local strategies applied before local definitive therapy, aiming to reduce tumor size and improve resectability [29]. Considering the aggressiveness of ES even a local approach may be meaningful also accounting that our research, extended to evaluating the biodistribution of GD2 CAR T cells post-administration, revealed their presence within the tumor site, and within a key immunological niche such as the spleen, indicating that a local injection of CAR T could potentially trigger a broader immunological response, as reported for other settings [30].

Advancing this approach towards a clinical trial in ES will benefit from further study in metastatic and recurrent models. Previously, strategies employing CAR-modified T or NK cells as a monotherapy have not always succeeded

in controlling ES models [18, 31, 32]. Ultimately, GD2 CAR T cells in ES may involve synergistic strategies with other chemotherapeutic and/or immunotherapeutic agents to boost CAR T cell efficacy. Combining GD2 CAR T cell therapy with an HGF receptor-neutralizing antibody has shown synergistic inhibition of tumor growth in orthotopic and metastatic disease models, where the antibody contributes to reducing tumor burden creating a more favorable microenvironment for adoptive cell therapy [31]. This underscores the significance of investigating synergistic or additive combination approaches with CAR T cell immunotherapy in the context of metastatic and recurrent ES, which still carries a dismal prognosis. In conclusion, this study validates the efficacy of GD2 CAR T cells in the treatment of ES, offering the potential to improve outcomes, at least for patients with localized disease.

Methods

Tumor cell culture maintenance and transduction

The human ES cell lines TC71 (RRID: CVCL_2213, DSMZ, Germany) and A673 (kind gift from Dr. Nicola Baldini, Rizzoli Orthopaedic Institute, Italy) were cultivated in Iscove's modified Dulbecco's medium (IMDM, Euroclone, Italy). RD-ES cell line (RRID: CVCL_2169, ATCC, LGC Standards S.r.l., Italy) was maintained in RPMI 1640 (Gibco, Thermo Fisher Scientific, USA). Media were supplemented with 10% FBS (Carlo Erba Reagents Srl, Italy), 1% L-glutamine (200 mM; BioWhittaker, Lonza, Belgium), and 1% penicillin-streptomycin (10^4 UI/ml penicillin and 10 mg streptomycin/ml; Carlo Erba Reagents Srl). The TC71 and A673 ES lines were engineered to express a firefly luciferase transgene using the RediFect™ Red-FLuc-Puromycin Lentiviral Particles (PerkinElmer, USA) and Firefly Luciferase Lentifect™ Purified Lentiviral Particles (GeneCopoeia, USA), respectively, according to the manufacturer's instructions. Photon emissions from the obtained luciferase-expressing TC71 (TC71 Luc) or A673 (A673 Luc) cells were measured using the IVIS Lumina XRMS (IVIS Lumina XRMS In Vivo Imaging System, PerkinElmer) with Living Image software (version 4.3.1, PerkinElmer), which was used to estimate the level of photon emission per cell. The TC71 and A673 ES lines were transduced by viral particles encoding for DsRed, as published [5]. The RD-ES cell line was engineered to stably express firefly luciferase and mScarlet using a third-generation lentiviral system. Briefly, the firefly luciferase and mScarlet transgenes were cloned into a pCCL-PGK-WPRE-based lentiviral backbone, to generate the bicistronic construct pCCL-PGK-Fluc-P2A-mScarlet-WPRE. The resulting transfer vector was transiently transfected into HEK293T packaging cells, together with the packaging plasmids, using GeneJuice (Sigma-Aldrich; #70967) transfection reagent. Conditioned medium containing lentiviral particles was collected 48 h post-transfection, filtered, snap-frozen, and subsequently used to transduce RD-ES cells seeded in 12-well plates (Corning, Kennebunk, ME, USA) with the addition of 6 µg/mL Polybrene. Transduction efficiency, measured by flow cytometry as the percentage of mScarlet-positive cells, remained above 99.9%, and therefore neither cell selection nor sorting was performed. ES cell lines were tested routinely for the absence of mycoplasma (MycoAlert Mycoplasma Detection Kit and MycoAlert Control Set, Lonza, Switzerland). The authentication of TC71, A673, and RD-ES cell lines was performed by the Leibniz Institute DSMZ - German Collection of Microorganisms and Cell Cultures GmbH.

CAR T cell manufacturing

CAR T cells were generated from peripheral blood mononuclear cells (PBMCs) isolated from anonymized buffy coats obtained from healthy blood donors ($n = 3$), as detailed in the Ethics statement. PBMCs were separated by a density gradient (Lymphoprep, Alere Technologies AS, Norway) and then resuspended in RPMI 1640 (Gibco) with 1% FBS, 1% glutamine and 1% penicillin-streptomycin. Non-adherent cells were pre-stimulated for 48 h in 7 µg/mL phytohemagglutinin (PHA-M, Sigma-Aldrich; #L8902) at a concentration of 1×10^6 cells/mL in a culture medium consisting of RPMI 1640 supplemented with 10% heat-inactivated defined FBS (Carlo Erba Reagents Srl, Italy), 500 UI/mL recombinant human Interleukin-2 (rhIL-2, Proleukin, Clinigen Healthcare Ltd, UK;). Isolated T lymphocytes

were transduced using a retroviral vector bearing second-generation anti-GD2 CAR (GD2 CAR; GD2.4-1BB.z) [20–22] and a Green Fluorescent Protein (GFP) control retroviral vector.

Flow cytometry

The expression of GD2 antigen on isolated tumor cells was assessed by flow cytometry. Primary unconjugated mouse anti-human GD2 (BD, Franklin Lakes NJ, USA; #554272, 1:20) and a secondary APC-conjugated goat anti-mouse Ig (APC Goat Anti-Mouse Ig polyclonal multiple adsorptions; BD; #550826, 1:20) were used for GD2 surface detection. Cells were also stained with the following antibodies for quantification of T cell subsets and memory phenotypes: iTCR/TCR γ/δ (APC, Biolegend, #331212), CD56 (PE, BD, #345812), CD3 (PerCP, BD, #345766 or FITC, BD, #349201), CD4 (PE, Biolegend, #345769), CD8 (PE-Cy7, Biolegend, #344750), CD45RA (APC, Biolegend, #304112), CCR7 (PerCP, Biolegend, #353219). Dilution of all the antibodies was 1:100. The transduction efficiency of GD2 CAR T and GFP T cells was determined by the percentage of GFP-positive cells. Data were collected by BD FACSAria III (BD) and BD FACSymphony A1 (BD) and analyzed using BD FACSDiva software (BD) and FlowJo ver. 10.8.2 software (BD).

Cytotoxicity assays in 2D

GD2 CAR T cells or GFP T cells were used as effectors (E) and human ES cell lines as targets (T). In vitro 2D co-cultures were established in 96-well plates (Corning, Kennebunk, ME, USA) at the effector-to-target (E:T) ratios of 1:1, 2:1, and 5:1. TC71 and A673 cells were seeded at a density of 7000 cells/well, while RD-ES cells were seeded at 10,000 cells/well. After 24 h, effectors were added at the indicated E:T ratios. For imaging purposes, lymphocytes were stained with calcein AM (0.175 µM; Thermo Fisher) before co-culture, and co-cultures were monitored over 72 hours using APEXVIEW APX100 Benchtop Fluorescence Microscope (Evident Scientific). The tumor bioluminescent signal after luciferin (150 µg/mL; XenoLight D-Luciferin-K^+ Salt; PerkinElmer) administration was quantified using the GloMax® Discover plate reader (Promega, Madison, WI, USA) as a measure of tumor cell viability at 24, 48, and 72 h. Cultures containing the medium alone or 1% Triton X-100 were used as controls, representing 100% and 0% cell viability, respectively. Average viability was calculated as 100 × (experimental bioluminescence − 0% viability bioluminescence)/(100% viability bioluminescence − 0% viability bioluminescence).

Automated single-cell killing assay

Single-cell killing assay was performed using the VivaCyte® platform (Cellply Srl, Bologna, Italy) with CC-Array® microfluidic devices (14 independent microchannels, 320 open-microwells/microchannel; 150 µm diameter per well). To support target cell adhesion, lower microchannels were pre-filled with 10:1 PDMS and polymerized in-situ. The resulting interface was functionalized with 15 µg/mL Fibronectin (Sigma-Aldrich; #F4759).

TC71 or A673 cells were stained with 7 µM CellTracker Blue CMAC (ThermoFisher; #C2110) and automatically seeded in the VivaCyte platform. After 24 h, GFP T or GD2 CAR T cells were stained with 175 nM Calcein-AM (ThermoFisher) and loaded into VivaCyte to establish co-cultures at the preferred effector-to-target ratio of 1:10. A solution of complete medium and propidium iodide (PI, visible in the TRITC band of VivaCyte; ThermoFisher; #P3566) was introduced in the CC-Array without cell displacement. The device was then maintained at 37 °C, 5% CO_2, and >90% humidity in the VivaCyte platform, with time-lapsed fluorescence imaging performed at 0, 4, 8, 12, and 24 h.

Images were analyzed via VivaCyte software using a deep learning model for effector cells detection. Single-effector analysis was performed by identifying microwells containing exactly one effector cell at 0 h; the mean PI signal intensity was then tracked over time to quantify the target cell death.

Cytotoxicity assays in 3D spheroid model

In vitro 3D cultures involved the formation of tumor spheroids. TC71, A673, and RD-ES spheroids were obtained by seeding 20,000 cells/well in a 96-well plate (Sphera Low-Attachment Surface, ThermoFisher). After 24 hours, ES spheroids were co-cultured with transduced lymphocytes at E:T ratios of 1:1, 2:1, and 5:1 over 3 days. For optical evaluation, lymphocytes were stained with calcein AM (0.175 µM; ThermoFisher) before co-culture. Co-cultures were monitored by APEXVIEW APX100 Benchtop Fluorescence Microscope over 72 h. The tumor bioluminescence was quantified using the GloMax® Discover plate reader (Promega) as a measure of tumor cell viability in the spheroid. Cultures containing only the medium, either stimulated with luciferin or not, were used as controls, representing 100% and 0% cell viability, respectively. Average viability was calculated as 100 × (experimental bioluminescence − 0% viability bioluminescence)/(100% viability bioluminescence − 0% viability bioluminescence).

ELISA

Supernatants were collected after 72 h of co-culture (E:T ratio 2:1) and cytokines (Granzyme B, perforin, IFNγ, TNFα) were quantified by the automated ELISA platform "Simple Plex ELLA" (ProteinSimple, Bio-Techne, Minneapolis, MN, USA). Instrument calibration was performed using the in-cartridge factory standard curve, and supernatant samples were diluted 1:2 in Sample Diluent (ProteinSimple).

In vivo studies

Animal experiments were pursued following approval by the National Ministry of Health and by the local Institutional Animal Care and Use Committee (Prot. N.22/2020-PR year). A total of 22 female and male 8–10-week-old NSG mice were obtained from Charles River (Charles River Laboratories Italia Srl, Lecco, Italy) and housed under a 12-h light, 12-h dark cycle with no restrictions on food and water. Sample size was estimated using tumor volume as the primary outcome measure and the software G*Power version 3.1.9.2 (Heinrich-Heine-University, Düsseldorf, Germany). No criteria were established for the inclusion or exclusion of animals in the study, and all animals were included in the subsequent analysis. Mice were fed a Teklad global purified rodent diet (2016) (Envigo, Indianapolis, Indiana, USA) to minimize potential signal interference during imaging analyses. Mycoplasma contamination was verified in supernatants of inoculated cells prior to in vivo use with a MycoALert Mycoplasma Detection Kit (Lonza Verviers, Belgium). 2.5×10^5 of TC71 Luc cells suspended into a mixture of 40 µL PBS and 40 µL Corning®Matrigel® (Merck Millipore, CLS354234-1EA) were injected subcutaneously at day −4. Four days after tumor cell inoculation, the animals were allocated to treatment groups using stratified randomization based on tumor volume and bioluminescence, ensuring balanced baseline average values and standard deviations for each parameter across groups. Group allocation was not performed in a blinded fashion. Treatment groups were three: the control group (CTR, $n = 6$) received 80 µL PBS; the GFP T cell group (GFP T, $n = 8$), and the GD2 CAR T cell group (GD2 CAR T, $n = 8$) received multiple ($n = 4$) intra/peri-tumoral injections consisting of 1.25 millions of GFP T cells and GD2 CAR T cells, respectively, at the first injection hit, followed by 2.0 millions for the subsequent three injections. To minimize potential confounders, animals were housed in separate cages according to their treatment groups after randomization. During data collection, cages were selected sequentially to analyze one group at a time. Animal health, weight and tumor volume were measured weekly. Animals were recurrently imaged using the IVIS Lumina XRMS (PerkinElmer) to detect the bioluminescent signal from TC71 Luc cells. For bioluminescence detection, 12 min after the subcutaneous injection of 150 mg/kg luciferin solution, the animals were anaesthetized with isoflurane (Merial, Lione, France) and imaged. Regions of interest were manually drawn around the tumor, and the total photon flux [p/s] emitted from tumor cells was quantified using Living Image software (PerkinElmer). A few tumor samples were dissociated to assess GD2 expression on tumor cells by flow cytometry, either immediately after dissociation or following one week of in vitro culture. Data were not analyzed in a blinded fashion.

Histology

For detection of GD2 expression, tumor samples were fixed in 4% PFA and washed with PBS before incubation with 30% sucrose PBS solution at 4 °C overnight, or until the tissue sank. Samples were then frozen on dry ice and stored at −80 °C until use. For cryo-sectioning, samples were placed in pre-labeled base plastic molds partially filled with frozen tissue matrix (OCT), completely covered with OCT compound, and allowed to solidify at −20 °C. Immunohistochemistry was performed on 8 µm-thick frozen sections blocked with 3% BSA (Bovine Serum Albumin) in PBS for 30 min at room temperature, followed by overnight incubation at +4 °C with a 1:100 dilution of mouse anti-GD2 primary antibody (BD, #554272) in 1% BSA in PBS. After rinsing, slides were incubated for 1 h at room temperature with an anti-mouse HRP-labeled secondary antibody (ThermoFisher, #31430) diluted 1:100. HRP activity was revealed using a 3.3 O-diaminobenzidine (DAB)-based kit (Sigma Aldrich, #D3939-1). For detection of GFP-expressing T cells, tumors were formalin-fixed, paraffin-embedded, and sectioned at 5 µm thickness. Sections were retrieved in citrate buffer (Sigma-Aldrich; #P2308) for 5 min at room temperature and incubated overnight at 4 °C with a primary rabbit anti-GFP antibody (Abcam, #AB290) at a dilution of 1:6000. Slides were then incubated for 1 hour at room temperature with a biotinylated goat anti-rabbit IgG (H + L) antibody at a dilution of 1:200 (Vector Laboratories, Burlingame, CA; #BA1000-1.5). Negative controls were processed concurrently by omitting the primary antibody and incubating with buffer only. Staining was developed using a DAB-based kit (Vector Laboratories; #SK-4100). All slides were counterstained with Harris hematoxylin (Bio Optica, Milan, Italy). All tumors were also evaluated by haematoxylin (Bio Optica, Milan, Italy) and eosin (Sigma-Aldrich) staining (H&E). Sections were examined by Zeiss Axioskop (Zeiss, Oberkochen, Germany) and by Nikon Eclipse Ci-L (Nikon Corporation, Tokyo, Japan). Photomicrographs were acquired by an AxioCam ICc3 color camera and AxioVision software (Zeiss).

Ethics

PBMCs were isolated from anonymized buffy coats obtained from healthy blood donors. Written informed consent for study participation, including the secondary use of anonymized residual samples for research purposes, was obtained from all donors by the providing institution. The use of these human-derived samples was approved by the Ethical and Institutional Review Board of the University Hospital of Modena (#318/2024_TESS CAR-T). All methods involving human-derived samples were performed in accordance with the relevant institutional guidelines and regulations and with the Declaration of Helsinki. All animal studies were conducted in accordance with the applicable institutional and national guidelines and under protocols approved by the Local Ethical Committee on Animal Experimentation and the Italian Ministry of Health (authorization no. 22/2020-PR).

Statistics

In vitro bioluminescence viability data were analyzed as repeated measures on the same samples, coming from three different donors. For each E:T ratio, linear mixed-effects models were fitted to evaluate the effects of treatment group (GFP T vs GD2 CAR T), time, and their interaction on the outcome variable (viability). Treatment group, time, and the interaction between group and time were included as fixed effects, whereas random intercepts were included for both sample and donors ID to account for within sample and repeated measure correlations. Models were fitted using restricted maximum likelihood (REML). Type III analysis of variance was performed on each mixed model using the Wald chi-square test to assess the significance of fixed effects and interactions. The obtained results were reported in terms of regression coefficients (mean differences, MD), with 95% Wald confidence intervals and p-values. The significance level alpha was set at 0.05. All analyses were carried out using R version 4.3.2 statistical software (The R Foundation for Statistical Computing).

For pairwise comparisons of cytokine release analyses, Wilcoxon–Mann–Whitney test was used. If the assumptions for parametric tests were met, the T-test was employed. P-values were adjusted using the Holm–Šídák method to account for multiple arms comparisons. For murine longitudinal analyses, a mixed-effects model with a Gamma

distribution and a logarithmic link function was estimated to deal with the non-linear association between outcomes and time. The model includes independent variables arm, time, and their interaction as fixed effects, while subject-specific intercept and slope terms were included as random effects. Adjusted *p*-values were considered significant when below the alpha level of 0.05. Statistical analyses were carried out using R Statistical software (The R Foundation for Statistical Computing) version 4.2.2 and GraphPad Prism Version 9.5.0 (525) for macOS. Graphs were created by GraphPad Prism Version 9.5.0 (525) for macOS and Adobe Illustrator 2023, all under a paid license.

Materials availability Materials used in this study are commercially available. Study-specific primary cell material can be provided upon availability and written request to the corresponding authors and signed material transfer agreement. Data can be made available upon request to the corresponding authors.

Supplementary information The online version contains supplementary material available at https://doi.org/10.1038/s41419-026-09268-x.

Acknowledgements We are extremely grateful to Prof. Dario Campana (Department of Pediatrics, Yong Loo Lin School of Medicine, National University of Singapore, Singapore) for the collaboration in developing the CAR receptor. We thank the Tecnopolo Mario Veronesi Mirandola and Fondazione Democenter for support and permission of using the IVIS Lumina XRMS. We thank CIGS ("Centro Interdipartimentale Grandi Strumenti" of the University of Modena and Reggio Emilia) for technical support when using Leica SP8 confocal microscopes. Dr. Flavia Parise, Prof. Renata Battini and Dr. Antonella Mauro (Animal Facility, University of Modena & Reggio Emilia) for technical support in the development of pre-clinical in vivo data. This work was supported in parts by the following grants: "Dipartimenti Eccellenti MIUR 2023-2027" (MS, MD), Diana Laneri post-doctoral fellowship 2021 (CC), Go4IT CRUI (GG), the Associazione ASEOP (MS), Donation in memory of Sara Lanfredi (LBrini), ASLEM (CC, MD), Donation in memory of Orazio Merighi (LBrini), and Fondazione Banco San Geminiano e San Prospero. The research leading to these results has received funding from the European Union - NextGenerationEU through the Italian Ministry of University and Research under PNRR - M4C2-I1.3 Project PE_00000019 "HEAL ITALIA" to MD and CC, CUP E93C22001860006. The views and opinions expressed are those of the authors only and do not necessarily reflect those of the European Union or the European Commission. Neither the European Union nor the European Commission can be held responsible for them. In the lasting memory of Marianna.

Author contributions GG, CC (co-first authors): conception and design of the study, data collection, drafting the manuscript, data analysis, interpretation, and data finalization; MP, MS, LBrini, GPugliese, GN, CS, RDT, LBertoni, GR, AM and MB: data collection, data analysis, and interpretation; TP, JV, and MCB: data collection. RCC and FB: statistical data analysis; GPalazzi, EMH, BLL: data interpretation; MD: conception and design of the work, drafting the manuscript, data analysis, interpretation, and data finalization. All authors critically reviewed the manuscript, and approved the final version.

Funding The funding sources played no role in the study design, data collection, data analysis, interpretation, writing of the report, and the decision of paper submission.

Data availability All data supporting the findings of this study are available within the paper.

Competing interests GG, CS, and MD hold patents in the field of cancer and gene therapy. AM is an employee of Cellply Srl. BLL is an inventor on patents and/or patent applications licensed to Novartis Institutes of Biomedical Research and receives license revenue from such licenses. BLL is an inventor on patents related to CAR therapy products and may be eligible to receive a portion of royalties paid from Kite (Gilead) to the University of Pennsylvania. BLL is a scientific co-founder and holds equity in Tmunity Therapeutics (acquired by Kite) and Capstan Therapeutics. BLL serves on the scientific advisory board of Avectas, Cellula, Edity Therapeutics, Immuneel, Immusoft, NeuCell Bio, Ori Biotech, Oxford Biomedica, Quell Therapeutics, and UTC Therapeutics. BLL is also on the board of directors of the Alliance for Cancer Gene Therapy. Conflicts of interest are managed in accordance with University of Pennsylvania policy and oversight.

Open Access This article is licensed under a Creative Commons Attribution 4.0 International License, which permits use, sharing, adaptation, distribution and reproduction in any medium or format, as long as you give appropriate credit to the original author(s) and the source, provide a link to the Creative Commons licence, and indicate if changes were made. The images or other third party material in this article are included in the article's Creative Commons licence, unless indicated otherwise in a credit line to the material. If material is not included in the article's Creative Commons licence and your intended use is not permitted by statutory regulation or exceeds the permitted use, you will need to obtain permission directly from the copyright holder. To view a copy of this licence, visit http://creativecommons.org/licenses/by/4.0/.

References

1. Grünewald TGP, Cidre-Aranaz F, Surdez D, Tomazou EM, de Álava E, Kovar H, et al. Ewing sarcoma. Nat Rev Dis Prim. 2018;4:5.
2. Tsibulnikov S, Fayzullina D, Karlina I, Schroeder BA, Karpova O, Timashev P, et al. Ewing sarcoma treatment: a gene therapy approach. Cancer Gene Ther. 2023;30:1066–71.
3. Setty BA, Gikandi A, DuBois SG. Ewing sarcoma drug therapy: current standard of care and emerging agents. Paediatr Drugs. 2023;25:389–97.
4. Grisendi G, Spano C, D'Souza N, Rasini V, Veronesi E, Prapa M, et al. Mesenchymal progenitors expressing TRAIL induce apoptosis in sarcomas. Stem Cells. 2015;33:859–69.
5. Golinelli G, Grisendi G, Dall'Ora M, Casari G, Spano C, Talami R, et al. Anti-GD2 CAR MSCs against metastatic Ewing's sarcoma. Transl Oncol. 2022;15:101240.
6. Finck AV, Blanchard T, Roselle CP, Golinelli G, June CH. Engineered cellular immunotherapies in cancer and beyond. Nat Med. 2022;28:678–89.
7. Albelda SM. CAR T cell therapy for patients with solid tumours: key lessons to learn and unlearn. Nat Rev Clin Oncol. 2024;21:47–66.
8. FDA Approves First Gene Therapy to Treat Adults with Metastatic Synovial Sarcoma. 2024. https://www.fda.gov/news-events/press-announcements/fda-approves-first-gene-therapy-treat-adults-metastatic-synovial-sarcoma.
9. Anastasiou M, Kyriazoglou A, Kotsantis I, Economopoulou P, Kyrkasiadou M, Giannopoulou A, et al. Immune checkpoint inhibitors in sarcomas: a systematic review. Immunooncol Technol. 2023;20:100407.
10. Machado I, López-Guerrero JA, Scotlandi K, Picci P, Llombart-Bosch A. Immunohistochemical analysis and prognostic significance of PD-L1, PD-1, and CD8+ tumor-infiltrating lymphocytes in Ewing's sarcoma family of tumors (ESFT). Virchows Arch. 2018;472:815–24.
11. Berghuis D, Santos SJ, Baelde HJ, Taminiau AH, Egeler RM, Schilham MW, et al. Pro-inflammatory chemokine-chemokine receptor interactions within the Ewing sarcoma microenvironment determine CD8(+) T-lymphocyte infiltration and affect tumour progression. J Pathol. 2011;223:347–57.
12. Stahl D, Gentles AJ, Thiele R, Gütgemann I. Prognostic profiling of the immune cell microenvironment in Ewing´s Sarcoma Family of Tumors. Oncoimmunology. 2019;8:e1674113.
13. Lin Z, Wu Z, Luo W. A novel treatment for Ewing's sarcoma: chimeric antigen receptor-T cell therapy. Front Immunol. 2021;12:707211.
14. Del Bufalo F, De Angelis B, Caruana I, Del Baldo G, De Ioris MA, Serra A, et al. GD2-CART01 for relapsed or refractory high-risk neuroblastoma. N Engl J Med. 2023;388:1284–95.
15. Majzner RG, Ramakrishna S, Yeom KW, Patel S, Chinnasamy H, Schultz LM, et al. GD2-CAR T cell therapy for H3K27M-mutated diffuse midline gliomas. Nature. 2022;603:934–41.
16. Nazha B, Inal C, Owonikoko TK. Disialoganglioside GD2 expression in solid tumors and role as a target for cancer therapy. Front Oncol. 2020;10:1000.
17. Kailayangiri S, Altvater B, Meltzer J, Pscherer S, Luecke A, Dierkes C, et al. The ganglioside antigen G(D2) is surface-expressed in Ewing sarcoma and allows for MHC-independent immune targeting. Br J Cancer. 2012;106:1123–33.
18. Kailayangiri S, Altvater B, Spurny C, Jamitzky S, Schelhaas S, Jacobs AH, et al. Targeting Ewing sarcoma with activated and GD2-specific chimeric antigen receptor-engineered human NK cells induces upregulation of immune-inhibitory HLA-G. Oncoimmunology. 2017;6:e1250050.
19. Liebsch L, Kailayangiri S, Beck L, Altvater B, Koch R, Dierkes C, et al. Ewing sarcoma dissemination and response to T-cell therapy in mice assessed by whole-body magnetic resonance imaging. Br J Cancer. 2013;109:658–66.
20. Prapa M, Caldrer S, Spano C, Bestagno M, Golinelli G, Grisendi G, et al. A novel anti-GD2/4-1BB chimeric antigen receptor triggers neuroblastoma cell killing. Oncotarget. 2015;6:24884–94.
21. Prapa M, Chiavelli C, Golinelli G, Grisendi G, Bestagno M, Di Tinco R, et al. GD2 CAR T cells against human glioblastoma. NPJ Precis Oncol. 2021;5:93.
22. Chiavelli C, Prapa M, Rovesti G, Silingardi M, Neri G, Pugliese G, et al. Autologous anti-GD2 CAR T cells efficiently target primary human glioblastoma. npj Precis Oncol. 2024;8:26.
23. Golinelli G, Grisendi G, Prapa M, Bestagno M, Spano C, Rossignoli F, et al. Targeting GD2-positive glioblastoma by chimeric antigen receptor empowered mesenchymal progenitors. Cancer Gene Ther. 2020;27:558–70.
24. Munoz-Garcia J, Jubelin C, Loussouarn A, Goumard M, Griscom L, Renodon-Cornière A, et al. In vitro three-dimensional cell cultures for bone sarcomas. J Bone Oncol. 2021;30:100379.
25. Casey DL, Lin TY, Cheung NV. Exploiting signaling pathways and immune targets beyond the standard of care for Ewing sarcoma. Front Oncol. 2019;9:537.
26. Sánchez-Molina S, Figuerola-Bou E, Sánchez-Margalet V, de la Cruz-Merino L, Mora J, de Álava Casado E, et al. Ewing sarcoma meets epigenetics, immunology and nanomedicine: moving forward into novel therapeutic strategies. Cancers. 2022;14:5473.

27. Majzner RG, Theruvath JL, Nellan A, Heitzeneder S, Cui Y, Mount CW, et al. CAR T cells targeting B7-H3, a Pan-cancer antigen, demonstrate potent preclinical activity against pediatric solid tumors and brain tumors. Clin Cancer Res. 2019;25:2560–74.
28. Flores G, Grohar PJ. One oncogene, several vulnerabilities: EWS/FLI targeted therapies for Ewing sarcoma. J Bone Oncol. 2021;31:100404.
29. Gaspar N, Hawkins DS, Dirksen U, Lewis IJ, Ferrari S, Le Deley MC, et al. Ewing sarcoma: current management and future approaches through collaboration. J Clin Oncol. 2015;33:3036–46.
30. Cherkassky L, Hou Z, Amador-Molina A, Adusumilli PS. Regional CAR T cell therapy: an ignition key for systemic immunity in solid tumors. Cancer Cell. 2022;40:569–74.
31. Charan M, Dravid P, Cam M, Audino A, Gross AC, Arnold MA, et al. GD2-directed CAR-T cells in combination with HGF-targeted neutralizing antibody (AMG102) prevent primary tumor growth and metastasis in Ewing sarcoma. Int J Cancer. 2020;146:3184–95.
32. Long AH, Highfill SL, Cui Y, Smith JP, Walker AJ, Ramakrishna S, et al. Reduction of MDSCs with all-trans retinoic acid improves CAR therapy efficacy for sarcomas. Cancer Immunol Res. 2016;4:869–80.

Publisher's note Springer Nature remains neutral with regard to jurisdictional claims in published maps and institutional affiliations.

Authors and Affiliations

Giulia Golinelli[1] · Chiara Chiavelli[1] · Malvina Prapa[2] · Marco Silingardi[1,3] · Leonardo Brini[1,4] · Giuseppe Pugliese[1] · Giovanni Neri[1] · Carlotta Spano[1] · Rosanna Di Tinco[5] · Laura Bertoni[5] · Riccardo Cuoghi Costantini[3,6] · Giulia Rovesti[1] · Alice Morellini[7] · Tiziana Petrachi[8] · Jonathan Vinet[9] · Marco Bestagno[10] · Maria Cristina Baschieri[1] · Federico Banchelli[6] · Giovanni Palazzi[11] · Edwin M. Horwitz[12] · Bruce L. Levine[13] · Massimo Dominici[1]

[1] Division of Oncology, Department of Medical and Surgical Sciences for Children & Adults, University-Hospital of Modena and Reggio Emilia, Modena, Italy

[2] Faculty of Medical Sciences, Albanian University, Tirana, Albania

[3] Clinical and Experimental Medicine PhD Program, University of Modena and Reggio Emilia, Modena, Italy

[4] Health Innovative Products and Technologies (HIP-TECH) PhD Program, Department of Life Sciences, University of Modena and Reggio Emilia, Modena, Italy

[5] Department of Surgery, Medicine, Dentistry and Morphological Sciences with Interest in Transplant, Oncology and Regenerative Medicine, University-Hospital of Modena and Reggio Emilia, Modena, Italy

[6] Center of Medical Statistic, Department of Medical and Surgical Sciences for Children and Adults, University-Hospital of Modena and Reggio Emilia, Modena, Italy

[7] Cellply Srl, Bologna, Italy

[8] Technopole "Mario Veronesi", Mirandola, Modena, Italy

[9] Centro Interdipartimentale Grandi Strumenti (CIGS), University of Modena and Reggio Emilia, Modena, Italy

[10] International Centre for Genetic Engineering and Biotechnology, Trieste, Italy

[11] Pediatric Unit, Azienda Ospedaliero-Universitaria Policlinico, Modena, Italy

[12] Department of Pediatrics, Emory University School of Medicine, Atlanta, GA, USA

[13] Center for Cellular Immunotherapies, University of Pennsylvania, Philadelphia, PA, USA

Edited by Professor Mauro Piacentini